Int. Journal of Refractory Metals and Hard Materials 47 (2014) 38–43

Contents lists available at ScienceDirect

Int. Journal of Refractory Metals and Hard Materials

journal homepage: www.elsevier.com/locate/IJRMHM

Effect of plastic deformation on the Σ2 grain boundary plane distribution in WC–Co cemented carbides

Xiaokun Yuan [a,*], Gregory S. Rohrer [b], Xiaoyan Song [a], Harry Chien [b], Jia Li [b], Chongbin Wei [c]

[a] College of Materials Science and Engineering, Beijing University of Technology, Beijing 100124, China
[b] Department of Materials Science and Engineering, Carnegie Mellon University, Pittsburgh, PA 15213-3890, USA
[c] Zhuzhou Cemented Carbide Cutting Tools Co. Ltd, Zhuzhou 412007, China

ARTICLE INFO

Article history:
Received 31 January 2014
Accepted 27 May 2014
Available online 2 June 2014

Keywords:
Cemented carbide
Plastic deformation
Σ2 grain boundary
Grain boundary plane distribution
Electron backscattered diffraction
Five parameter analysis

ABSTRACT

Grain boundary plane distributions have been measured for Σ2 grain boundaries (boundaries that have a 90 degree rotation about the [10-10] axis) in undeformed and plastically deformed WC–Co cemented carbides. By virtue of electron backscattered diffraction data coupled with the five parameter analysis method, the measurements show that while the misorientations of the Σ2 boundaries are 20% reduced by the plastic deformation, there are 33% reduction in the orientation of the Σ2 twist grain boundary plane. A dislocation model for grain boundary plane reorientation during plastic deformation is proposed.

Introduction

Cemented carbides, which generally comprise hard tungsten carbide phases embedded in tough metallic binder phases, have outstanding mechanical properties and are widely used where hardness and erosion/abrasion resistance are essential. In the polycrystalline microstructure of WC–Co cemented carbides, the crystals are joined at internal interfaces including WC/WC grain boundaries, Co/Co grain boundaries, and WC/Co phase boundaries. Among these boundaries, one of the most frequently occurring WC/WC boundaries can be described as a 90 degree rotation about the [10-10] axis and is abbreviated as 90°/[10-10] boundary [1]. In coincidence site lattice (CSL) notation, this boundary is referred to as Σ2 boundary, where the low Σ value represents a high reciprocal density of coinciding sites and a symmetrical configuration of dense planes [2]. The boundary is also thought to have a low interfacial energy and high work of separation [3]. Note that the c/a ratio of WC is 0.976, so the Σ2 boundary is actually an "approximate" or "near" CSL boundary.

Typical WC–Co cemented carbides usually contain 6–15 wt.% cobalt as the binder phase and hence, the properties of the material are closely related to the composition and polycrystalline structure. In characterizing the polycrystalline microstructure of cemented carbides, grain boundary plane crystallography should not be neglected because the mesoscale structure of the grain boundary network can influence the performance and integrity of the material [4]. Recently, a stereological approach named "five parameter analysis (FPA)" has been developed to calculate grain boundary plane distributions (GBPDs) from electron backscattered diffraction (EBSD) data [5]. Using this method, the grain boundary distribution is expressed in terms of five macroscopically observable parameters, including three Eulerian angles to describe the lattice misorientation across the boundary and two spherical angles to describe the orientation of the grain boundary plane normal. Thus, the FPA provides a more comprehensive description of the grain boundaries within a polycrystal. The utility of the FPA method for measuring the Σ2 grain boundary population in WC–Co cemented carbides has been described in several recent publications [6–11].

Plastic deformation is one significant process that occurs in the application of cemented carbides. For example, it has been reported that plastic deformation limits the performance of cemented carbide tools, especially under high load conditions [12]; moreover, the accumulation of plastic deformation can affect either the fragmentation behavior of WC grains [13], or the distribution of residual stresses in the microstructure of the material [14]. Therefore, how plastic deformation influences the distribution of Σ2 grain boundaries is an important question that needs more attention. Accordingly, the objective of the present work is to compare the GBPD for Σ2 boundaries in two samples that are nominally the same, except that one has been subjected to plastic deformation to represent the load conditions when cemented carbides are used in practice. As a consequence, the results provide beneficial information about how plastic deformation affects the population as well as the plane distribution of Σ2 grain boundaries.

* Corresponding author. Tel.: +86 10 67396260.
E-mail address: yuanxiaokun@bjut.edu.cn (X. Yuan).

http://dx.doi.org/10.1016/j.ijrmhm.2014.05.012
0263-4368/

Experimental

The two cemented carbide samples used in this work have a cobalt fraction of 8 wt.% and no intentional alloying additions. The specimens were prepared in the same batch by sintering in a hot isostatic press (sinter-HIP) with a 6 MPa argon atmosphere and a nominal sintering temperature of 1500 °C maintained for 60 min, which gives the samples an average grain size of about 1 μm. Sample 1 (similarly hereinafter), which was not deformed, is used as a reference. Sample 2 (similarly hereinafter) was subjected to plastic deformation via a MTS 810 material test machine. Specifically, sample 2 was deformed in a controlled three-point bending strength measurement. The procedure was performed with a test span of 14.5 ± 0.5 mm and a loading speed of 200 N/min. The measurement indicated that sample 2 had a transverse rupture strength of 2970 MPa. From this sample, a volume of material close to the most heavily deformed zone was extracted for further examination.

The two samples were then treated for EBSD analysis by polishing with a diamond abrasive and etching in Murakami's reagent (1 g potassium + 1 g sodium + 10 ml distilled water) for no more than 5 s. This treatment yielded WC surfaces suitable for EBSD mapping. The EBSD measurements were then performed by a high speed EBSD detector incorporated in a Zeiss Supra 55 scanning electron microscope (SEM). To ensure the accuracy of the measurements, the data were recorded with a step size of 0.08 μm.

The obtained EBSD data sets then [1–6] underwent a phase clean procedure and then were exported to the EDAX OIM Analysis 5.31 software for processing. The first step in EBSD data processing was to use a cleanup procedure to correct spurious points in the orientation map that arise from incorrect indexing [1–6]. Grain dilation with a minimum grain size of 4 pixels followed by neighbor orientation correlation in the OIM software was used as the data cleanup procedure, and such procedure ensures the reliable orientation assignments for small grains. As a consequence, the maximum fraction of pixels cleaned due to the cleanup procedure was approximately 5% in both samples. Afterwards, the microtexture and misorientation statistics represented by the boundary length fraction were derived from the OIM software. The Brandon criterion was used to determine the fraction of Σ2 boundaries [15]. The observations needed for the FPA analysis are line segments that are extracted from the orientation maps according to the misorientation across the boundary and are associated with the crystal orientations. The grain boundary plane distribution for the Σ2 boundaries was calculated using programs developed at Carnegie Mellon University that contain a stereological procedure coupled with an automated trace analysis step. The procedure for doing this is described in reference [5]. Using the FPA method, the grain boundary distribution, $\lambda(\Delta g,n)$, is defined as the relative area of a grain boundary with a misorientation, Δg, and boundary plane normal, n, in units of multiples of a random distribution (MRD).

To make the comparison between GBPDs of the undeformed and deformed samples convincing, several issues need to be addressed. First, consistent with references [12,13], the diffraction patterns from the deformed sample were observed to be of lower quality than from the undeformed sample. Considering this, measurement regions with relatively low deformation were preferentially selected where the diffraction patterns were not significantly degraded. In other words, regions of the deformed sample where most pixels were correctly indexed were used. This ensures the precision of the method and makes it reasonable to compare the GBPDs of the two samples [1–4]. Second, the precision in determining the grain boundary traces for the two samples (especially for the deformed sample) is acceptable in the present work. Note that the average grain size is about 1 μm in both samples, while the step size is 0.08 μm, so each grain edge is, on average, defined by 12.5 pixels, and a 0.08 micron step in the middle of a 1 micron line segment would maximally induce a deviation angle of 4.6°, which is below the tolerance angle of 5° to determine the grain orientations in the current work. Third, the FPA method requires a sufficient number of boundary traces to reliably determine the GBPD. Tungsten carbide has a hexagonal space group ($P\bar{6}m2$), and for this symmetry, 2×10^5 boundary traces are required to determine the five-dimensional distribution of interfaces [5]. Also, 2×10^3 boundary traces are needed to determine the two-dimensional distribution of habit planes if the three misorientation parameters are ignored. In other words, $\lambda(\Delta g,n)$ represents the GBPD in a five-dimensional space, and $\lambda(n)$ represents GBPD in a two-dimensional space [5]. In this work, more than 2×10^5 grain boundary traces were recorded on each sample, so the GBPD is statistically reliable.

Results

The microstructures of the two samples are illustrated by the image quality (IQ) maps in Fig. 1, with Σ2 boundaries highlighted in red. IQ maps are used to represent variations in the quality of EBSD patterns in a given area. The image quality is lower for diffraction patterns obtained near grain boundaries; that is to say, the quality of the diffraction patterns is not good at boundaries and probably even worse at boundaries in the deformed sample where dislocations might concentrate. Both samples exhibit microstructures with a continuous skeleton of prismatic WC grains embedded in the cobalt binder phase [1,2]. Note that IQ maps in Fig. 1 cannot sufficiently represent the grain size distributions in each sample. Actually, both samples have an average carbide

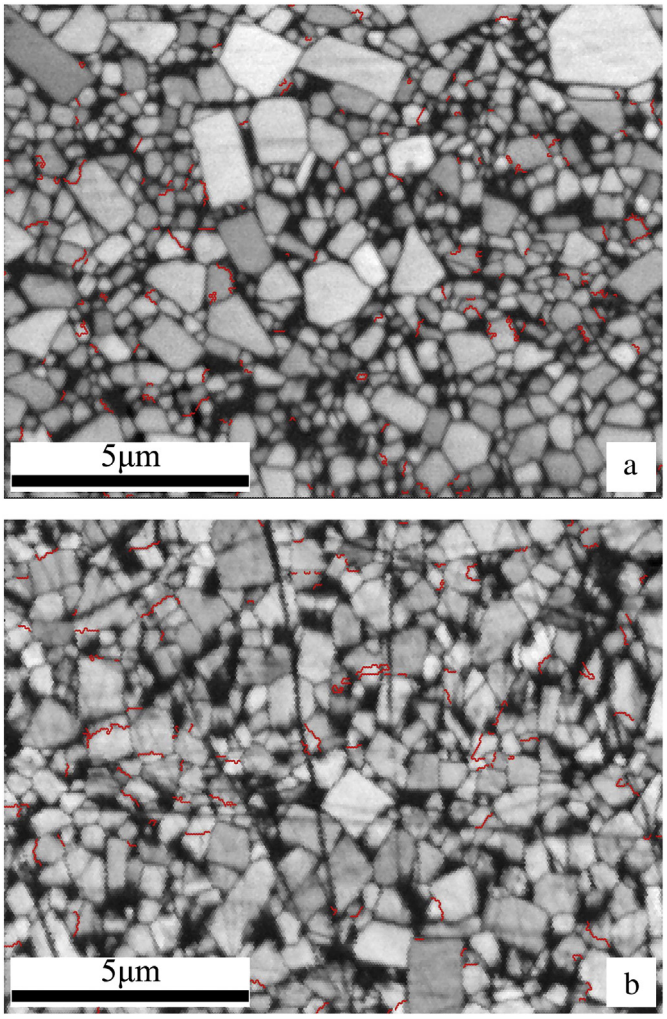

Fig. 1. Image quality maps of typical measurement regions, with Σ2 grain boundaries highlighted in red, (a) sample 1; (b) sample 2. (For interpretation of the references to color in this figure legend, the reader is referred to the web version of this article.)

grain size of about 1 μm, and the grain size distributions in the two samples are quite similar [1–5]. Also note that the slight scratches in Fig. 1(b) merely cause limited decrease of EBSD pattern quality and such scratches therefore cannot obviously influence the indexing of carbide grains as well as Σ2 grain boundaries.

The main concern of this work is the orientation texture of the WC/WC grain boundary planes at boundaries with the Σ2 misorientation. As the first step, to analyze the orientation relationship between WC grains, the misorientation angle distribution was calculated and the outcome is shown in Fig. 2. In the chart, the black line represents the misorientation distribution for an ideally random microstructure, while the blue and red lines show the misorientation distributions for the grain boundaries in samples 1 and 2, respectively. It can be seen that the experimental distributions are clearly not random. Two misorientation angle preferences, corresponding to the sharp peaks at 30° and 90°, were observed. Furthermore, the peak at 90° for sample 2 is 21% lower than for sample 1. The misorientation distributions in the two samples are nearly the same, indicating that plastic deformation does not remarkably influence the misorientation angle preferences between WC grains.

As the next step, to examine the distribution of misorientation axes, the data are plotted in the axis–angle space. As illustrated in Fig. 3, in each layer of the axis–angle space, all possible axes are represented, and the rotation angle varies along the vertical direction. Larger values indicate relatively stronger preference of that axis and angle. Note that at the position close to 30°, there is a peak at the [0001] rotation axis. This could represent a relatively high coincidence CSL boundary (27.796°/[0001] or Σ13a boundary [1]), which has high interface coincidence in the twist configuration. There is an even larger deviation from random for rotations of 90°, with a strong peak at the [10-10] rotation axis, indicating that [10-10] is the dominant misorientation axis, and boundaries with such misorientation occur most frequently. In this paper, we mainly focus the analysis on the 90°/[10-10] or Σ2 boundary. By comparing the maximum at the Σ2 position, we can estimate that there is a 20% reduction in the number of these boundaries. The number and length fractions of Σ2 grain boundaries in the two samples, calculated using a 5° tolerance, are listed in Table 1. Both results confirm that the Σ2 population is decreased as a result of plastic deformation.

Two possible configurations for the Σ2 boundary are a twist boundary where the interface consists of (10-10) prismatic planes in both grains, and a tilt boundary consisting of a (0001) basal plane in one grain against a (10-10) prismatic plane in the other, as shown in Fig. 4. In each chart, there are two artificially drawn hexagonal crystals

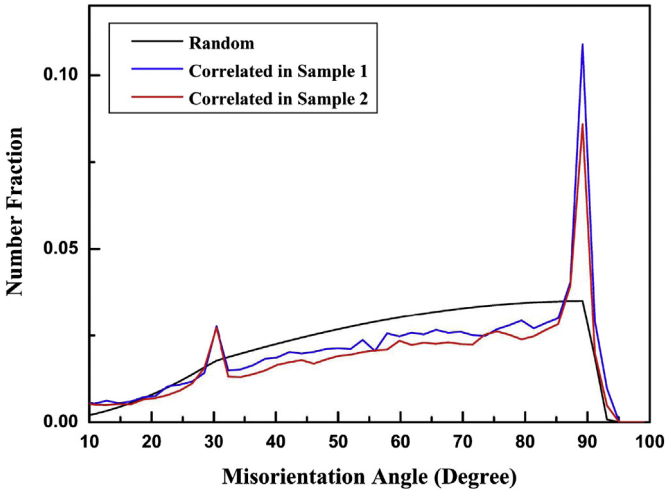

Fig. 2. The distribution of grain boundary misorientations for the two samples and the distribution expected for randomly oriented objects, as a function of misorientation angle. (For interpretation of the references to color in this figure, the reader is referred to the web version of this article.)

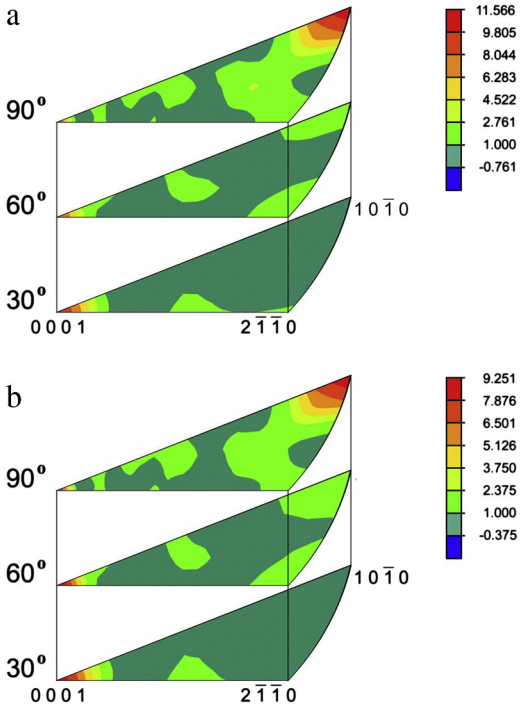

Fig. 3. WC/WC grain boundary misorientation distribution in axis–angle space. Three sections of the fundamental zone are taken perpendicular to the [0001] axis, with units of the contours in MRD, (a) sample 1; (b) sample 2. (For interpretation of the references to color in this figure legend, the reader is referred to the web version of this article.)

consistent with the lattice orientations measured by the OIM software, which are imposed on the image to indicate the orientation of the grains across a certain Σ2 grain boundary. However, without further analysis, conventional methods cannot distinguish between these two possibilities. Nevertheless, by examining two-dimensional sections of the five parameter GBPD, it is possible to compare the grain boundary plane distribution at specific misorientations. The misorientation distribution (see Fig. 3) can be used as a guide for the selection of appropriate sections. After a misorientation is chosen, the corresponding plane area distribution for that misorientation is plotted in a stereographic projection. For the two samples in this work, the grain boundary plane distributions for the Σ2 boundaries are presented in Fig. 5.

In Fig. 5, the grain boundary plane distribution is the relative areas of different grain boundary planes at the misorientation of 90° about [10-10]. For both samples, the peak of the distribution is at the position of the corresponding misorientation axis, [10-10], which means that the boundary plane is perpendicular to the common rotation axis of the grain pair; that is to say, the boundary has a pure twist configuration. The absence of a peak along the great circle perpendicular to the misorientation axes indicates that tilt boundaries are not common at this misorientation. The relative area of Σ2 twist boundaries in sample 1 (240 MRD) and sample 2 (160 MRD) indicates that plastic deformation reduces the populations of these boundaries by a factor of about one third, which is greater than the reduction when calculated by the misorientation alone (about 20% using the data in Table 1). This indicates that for some of the bicrystals, the grain boundary plane is rotated while the misorientation is maintained.

SEM images would be helpful to visualize the effect of plastic deformation, for example, to show whether there are slip line traces in the microstructure. An example of this can be found in reference [13]. However, the change in the orientation texture of the boundary planes that results from plastic deformation is relatively difficult to determine from an SEM image. To complement the five-dimensional distribution of boundary planes presented in Fig. 5, the two-dimensional distribution of carbide/carbide boundary planes (ignoring misorientation parameters)

Table 1
Statistics for grain boundaries in the samples.

	Sample 1 (undeformed)	Sample 2 (deformed)
Number fraction of Σ2 grain boundary (%)	7.0	6.6
Length fraction of Σ2 grain boundary (%)	12.7	10.6
Number of WC/WC grain boundary segments per micron square	2.93	4.79
Number of WC/Co phase boundary segments per micron square	3.98	7.37
Number of triple junctions (of boundary segments) per micron square	6.25	8.42

of the two samples is also provided in Fig. 6. The figures show that the (0001) basal plane and (10-10) prismatic planes at carbide/carbide grain boundaries occur with different frequencies (measured in units of MRD) in the two samples; moreover, the decrease in the population of (10-10) prismatic planes (1.40 MRD for sample 1 and 1.30 MRD for sample 2) is consistent with the decrease of the relative area of Σ2 twist boundaries after plastic deformation (see Fig. 5). Therefore, it can be concluded that the grain boundary plane distribution is altered by plastic deformation.

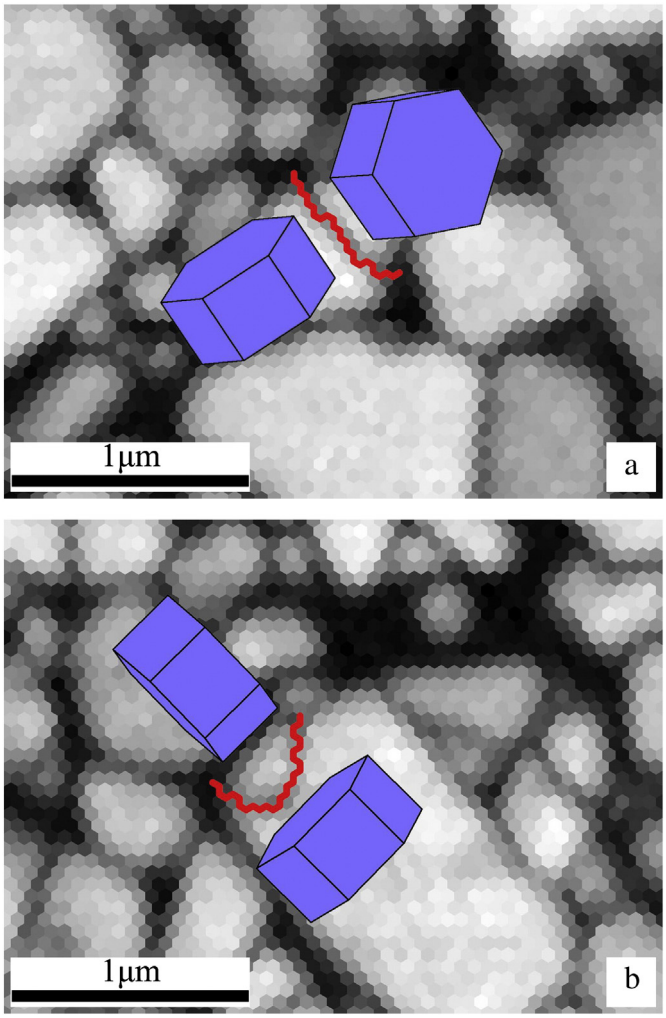

Fig. 4. Structures of the Σ2 twist (a) and tilt (b) boundaries. (For interpretation of the references to color in this figure legend, the reader is referred to the web version of this article.)

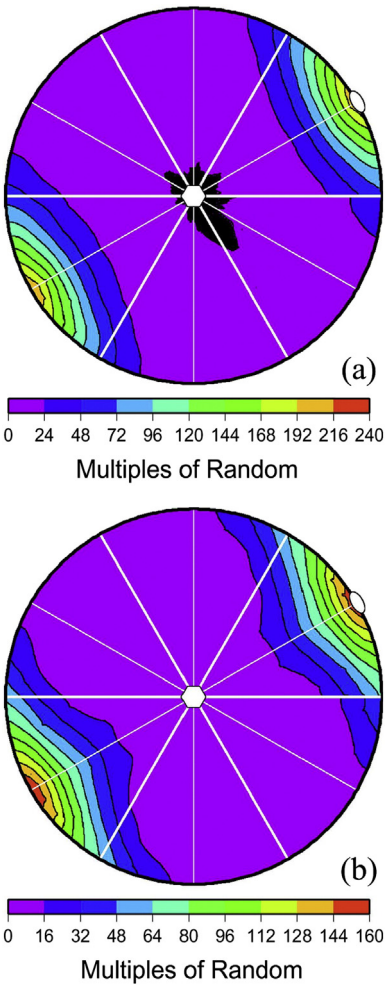

Fig. 5. Grain boundary plane distributions of Σ2 boundaries. The locations corresponding to the (0001) and (10-10) orientations are indicated by hexagons and ovals, respectively, and the units of the contours are MRD, (a) sample 1; (b) sample 2. (For interpretation of the references to color in this figure legend, the reader is referred to the web version of this article.)

Discussion

The change in the grain boundary plane distribution that results from plastic deformation could have several possible origins: grain boundary sliding [16], grain boundaries being separated and infiltrated with binder [3], grain rotations resulting from dislocation accumulation [17], and grain shape changes associated with dislocation motion. Grain boundary sliding parallel to the grain boundary plane would reduce the total area of Σ2 boundaries by reducing the total area of contact. This could account for the change in the misorientation distribution, as shown in Table 1, but it would not result in the reorientation of the grain boundary plane. To determine whether the opening of the boundary and infiltration of the grain boundary plane is plausible, one can consider the energy of the interface. In reference [12], ab initio calculations were used to determine the energy of Σ2 grain boundaries; the results indicate that the interface energy of the Σ2 twist boundary is two orders of magnitude lower than the energy of the Σ2 tilt boundary. This is consistent with the fact that Σ2 twist boundaries are the most common and that there are very few Σ2 tilt boundaries. However, it also means that the Σ2 twist boundary is unlikely to separate and be infiltrated by the binder. Even if separation were occurring, it would decrease the total fraction of Σ2 boundaries rather than cause the reorientation of the grain boundary planes at the same misorientation. Grain orientations can also rotate during deformation, either by dislocation

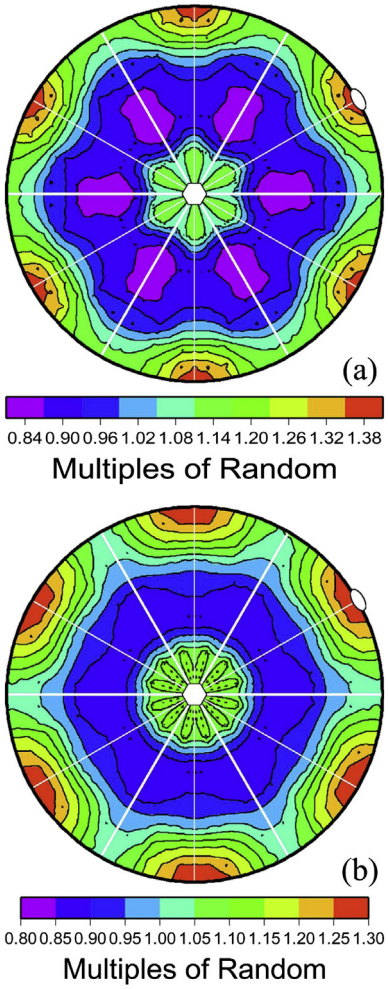

Fig. 6. Grain boundary plane distributions of carbide/carbide boundary planes. The locations corresponding to the (0001) and (10-10) orientations are indicated by hexagons and ovals, respectively, and the units of the contours are MRD, (a) sample 1; (b) sample 2. (For interpretation of the references to color in this figure legend, the reader is referred to the web version of this article.)

accumulation or coupled rigid body motions. While these processes can change the number of Σ2 boundaries, it would affect the misorientation and the boundary plane orientation equally. Therefore, to provide a plausible explanation for how the Σ2 grain boundary plane orientations are altered more than the misorientation, we turn to a consideration of grain shape changes associated with dislocation motion.

When dislocations pass through a crystal, both steps and residual dislocation content might be generated in the boundary [17]. In the context of this work, the consequence of steps generated by dislocation motion is that it changes the external shape of a crystal, without changing its crystallographic orientation with respect to an external reference frame. However, the shape change amounts to an alteration of the orientations of the external surfaces with respect to the crystal reference frame. One can imagine a similar process occurring in a bicrystal, as long as the dislocation can pass out of one crystal, through the grain boundary, and then through the second crystal. This will result in the reorientation of the grain boundary plane. In WC, plastic deformation might occur via the glide of dislocations by various slip systems [12,16,18]. In this work, we focus the <0001>{10-10} slip system reported in reference [16]. For a Σ2 twist grain boundary, there are no parallel slip planes, so direct dislocation transmission cannot occur. However, three {10-10} planes intersect in this boundary along a line in the (0001) plane of the second crystal (another slip system), so that the cross slip of dislocations across the boundary is possible.

We should note that the same phenomenon is not expected to occur at general boundaries. In lower symmetry boundaries, there is a much smaller probability that slip planes will intersect and permit cross slip. In this case, dislocations are expected to pile up at the interface, and eventually, the accumulation of dislocations by this mechanism will lead to lattice curvature and rotation. This is consistent with the findings in reference [13], which reported that in deformed WC, EBSD patterns were degraded and the orientation rotated compared to the undeformed region. Similar rotations and reorientations should have occurred in the sample studied here. Preliminary evidence for this is the increase in the number of various interfaces per unit area of the plane sections; see the statistical results in Table 1.

Conclusions

In summary, the FPA method has been used to compare the grain boundary plane distributions for the Σ2 grain boundary in undeformed and plastically deformed WC–Co samples. While the plastic deformation made a 20% reduction on the fractional population of grain boundaries with the Σ2 misorientation, the fraction of Σ2 twist type boundaries was one third lower. The reorientation of the grain boundary plane could be caused by the cross slip of dislocation through the interface plane.

Acknowledgments

GSR acknowledges support from Office of Naval Research Grant N00014-11-1-0678. Facilities support from the Carnegie Mellon MRSEC, under the National Science Foundation under Award Number DMR-0520425, are also acknowledged. Xiaoyan Song acknowledges support from the National Natural Science Foundation of China 51174009. Xiaokun Yuan acknowledges supports from the Beijing Natural Science Foundation 2123061 and the State Key Lab of Advanced Metals and Materials 2013-Z01. Xiaokun Yuan is grateful to several anonymous experts for their valuable comments and suggestions, including the concern about the experimental procedure and precision of the method. Xiaokun Yuan appreciates Prof. Weiguo Wang from Fujian University of Technology, Prof. Ping Yang form University of Science and Technology Beijing, Dr. Xiaoying Fang from Shandong University of Technology, for giving important insights to this work since Year 2010. Xiaokun Yuan also appreciates Dr. Ken P. Mingard from the National Physical Laboratory, UK for the fruitful discussion, and appreciates Dr. Yuntao Lei for providing kind help to this work. Dr. Hongmei Xu is also thanked for giving linguistic advice.

References

[1] Hagege S, Nouet G, Delavignette P. Grain boundary analysis in TEM (IV): coincidence and the associated defect structure in tungsten carbide. Phys Status Solidi A 1980;62:97–107.
[2] Vicens J, Benjdir M, Nouet G, Dubon A, Laval JY. Cobalt intergranular segregation in WC–Co composites. J Mater Sci 1994;29:987–94.
[3] Christensen M, Wahnstrom G. Co-phase penetration of WC(10-10)/WC(10-10) grain boundaries from first principles. Phys Rev B 2003;67:115415.
[4] Rohrer GS. Measuring and interpreting the structure of grain-boundary networks. J Am Ceram Soc 2011;94:633–46.
[5] Saylor DM, Dasher BS, Adams BL, Rohrer GS. Measuring the five-parameter grain boundary distribution from observations of planar sections. Metall Mater Trans A 2004;35:1981–9.
[6] Kim CS, Rohrer GS. Geometric and crystallographic characterization of WC surface and grain boundaries in WC–Co composites. Interface Sci 2004;12:19–27.
[7] Kim CS, Massa TR, Rohrer GS. Interface character distributions in WC–Co composites. J Am Ceram Soc 2008;91:996–1001.
[8] Yuan XK, Song XY, Chien H, Li J, Rohrer GS. Effect of densification mechanism on the Σ2 grain boundary plane distribution in WC–Co composites. Mater Lett 2013;92:86–9.
[9] Yuan XK. Grain boundary character distributions of coincidence site lattice boundaries in WC–Co composites with different WC grain sizes. J Alloys Compd 2013;579:622–7.
[10] Yuan XK. Grain boundary character distributions of sigma2 boundaries in WC–Co composites with different cobalt volume fractions. Ceram Int 2014;40:1873–8.
[11] Yuan XK, Rohrer GS, Song XY, Chien H, Li J. Modeling the interface area aspect ratio of carbide grains in WC–Co composites. Int J Refract Met Hard Mater 2014;44:7–11.

[12] Ostberg G, Farooq MU, Christensen M, Andren HO, Klement U, Wahnstrom G. Effect of Σ2 grain boundaries on plastic deformation of WC–Co cemented carbides. Mater Sci Eng A 2006;416:119–25.
[13] Gee M, Mingard KP, Roebuck B. Application of EBSD to the evaluation of plastic deformation in the mechanical testing of WC/Co hardmetal. Int J Refract Met Hard Mater 2009;27:300–12.
[14] Roebuck B, Klose P, Mingard KP. Hardness of hexagonal tungsten carbide crystals as a function of orientation. Acta Mater 2012;60:6131–43.
[15] Brandon DG. The structure of high-angle grain boundaries. Acta Metall 1966;14:1479–84.
[16] Bolton JD, Redington M. Plastic deformation mechanisms in tungsten carbide. J Mater Sci 1980;15:3150–6.
[17] Pond RC, Serra A, Bacon DJ. Dislocations in interfaces in the h.c.p. metals—II. Mechanisms of defect mobility under stress. Acta Mater 1999;47:1441–53.
[18] Vicens J, Pinson EL, Chermant JL, Nouet G. Structural analysis and properties of grain boundaries in hexagonal carbides. J Phys 1988;49:271–6.